Mispairing of the 8,9-Dihydro-8-(N7-guanyl)-9-hydroxy-aflatoxin B_1 Adduct with Deoxyadenosine Results in Extrusion of the Mismatched dA toward the Major Groove†

Indrajit Giri, David S. Johnston, and Michael P. Stone*

Department of Chemistry and Center in Molecular Toxicology, Vanderbilt University, Nashville, Tennessee 37235

Received December 4, 2001; Revised Manuscript Received February 11, 2002

ABSTRACT: The G → T transversion is the dominant mutation induced by the cationic *trans*-8,9-dihydro-8-(N7-guanyl)-9-hydroxy-aflatoxin B_1 adduct. The structure of d(ACATC^{AFB}GATCT)·d(AGATAGATGT), in which the cationic adduct was mismatched with deoxyadenosine, was refined using molecular dynamics calculations restrained by NOE data and dihedral restraints obtained from NMR spectroscopy. Restrained molecular dynamics calculations refined structures with pairwise rmsd <1 Å and a sixth root R_1^x factor between the refined structure and NOE data of 10.5×10^{-2}. The mismatched duplex existed in a single conformation at neutral pH. The aflatoxin moiety intercalated above the 5′ face of the modified ^{AFB}G. The mismatched dA was in the anti conformation about the glycosyl bond. It extruded toward the major groove and did not participate in hydrogen bonding with ^{AFB}G. The structure was compared with that of d(ACATCGATCT)·d(AGATAGATGT) containing the corresponding unmodified G·A mismatch and with d(ACATC^{AFB}GATCT)·d(AGATCGATGT) containing the aflatoxin lesion in the correctly paired ^{AFB}G·C context. The correctly paired oligodeoxynucleotide exhibited Watson−Crick-type geometry at the ^{AFB}G·C pair. It melted at higher temperature than the mismatched ^{AFB}G·A duplex. The unmodified mismatched G·A duplex exhibited spectral line broadening at neutral pH, suggesting a mixture of conformations. It exhibited a lower melting temperature than did the mismatched ^{AFB}G·A duplex. These differences correlated with replication bypass experiments performed in vitro utilizing DNA polymerase I *exo*- [Johnston, D. S., and Stone, M. P. (2000) *Chem. Res. Toxicol. 13*, 1158−1164]. Those experiments showed that correct insertion of dC opposite ^{AFB}G blocked replication by the enzyme, whereas incorrect insertion of dA opposite ^{AFB}G allowed full-length replication of the adducted template strand.

Aflatoxin B_1 (AFB_1)[1] is the predominant mutagenic metabolite which is isolated from several species of the genus *Aspergillus*. This mycotoxin is of worldwide health concern because of the potential contamination of the food supply (*1*). AFB_1 is a mutagen in bacteria (*2*−*4*); it is carcinogenic in fish (*5*, *6*), and it is a hepatocarcinogen in rodents (*7*, *8*). It is linked to the etiology of human liver cancer (*1*) possibly via adduct-induced mutations in the p53 tumor suppresser gene (*9*−*15*) and *ras* protooncogenes (*7*, *8*) and probably exacerbated by co-infection by the hepatitis B virus (*14*, *16*−*18*).

AFB_1 is primarily metabolized in humans by cytochrome P_{450} 3A4 (*19*) to yield AFB_1-*exo*-8,9-epoxide (*20*, *21*). The *exo*-epoxide bonds to the N7 position of guanine to yield *trans*-8,9-dihydro-8-(N7-guanyl)-9-hydroxy-aflatoxin B_1 (*22*) (Scheme 1). The regioselectivity of adduction is consistent with the precovalent intercalation of the epoxide on the 5′ face of guanine (*23*−*28*) that places the epoxide in close proximity and in the proper orientation to the N7 position of guanine, thus facilitating a back side S_N2 reaction (*29*). Site-specific mutagenesis indicates that the *trans*-8,9-dihydro-8-(N7-guanyl)-9-hydroxy-aflatoxin B_1 adduct is an efficient mutagenic lesion (*30*, *31*). Overall, it seems likely that AFB_1 is an important contributor to human cancer.

Some years ago, NMR studies revealed that the *trans*-8,9-dihydro-8-(N7-guanyl)-9-hydroxy-aflatoxin B_1 adduct intercalated above the 5′ face of the modified guanine in two oligodeoxynucleotides: d(ATC^{AFB}GAT)·d(ATCGAT) and d(AT^{AFB}GCAT)$_2$ (*32*). The structurally related guanine N7 sterigmatocystin adduct formed a similar intercalated structure (*33*). More recently, the solution structures of the

† This work was supported by NIH Grant CA-55678 (M.P.S.). Funding for the 500 MHz NMR spectrometer was supplied by NIH Grant RR-05805. Additional funding for NMR instrumentation was provided by Vanderbilt University and the Vanderbilt Center in Molecular Toxicology, Grant ES-00267.

* To whom correspondence should be addressed. Phone: (615) 322-2589. Fax: (615) 322-4936. E-mail: stone@toxicology.mc.vanderbilt.edu.

[1] Abbreviations: AFB_1, aflatoxin B_1; EDTA, ethylenediaminetetraacetic acid; HPLC, high-pressure liquid chromatography; NOE, nuclear Overhauser enhancement; NOESY, two-dimensional nuclear Overhauser enhancement spectroscopy; ppm, parts per million; MD, molecular dynamics; rMD, restrained molecular dynamics; PEM, potential energy minimization; rmsd, root-mean-square deviation; TPPI, time-proportional phase increment; 1D, one dimensional; 2D, two dimensional. The oligodeoxynucleotides discussed in this paper do not have terminal phosphate groups; we abbreviate the nomenclature for oligodeoxynucleotides by leaving out the phosphodiester linkage. A, C, G, and T refer to mononucleotide units; ^{AFB}G refers to the *trans*-8,9-dihydro-8-(N7-guanyl)-9-hydroxy-aflatoxin B_1 adduct. A right superscript refers to the numerical position in the oligodeoxynucleotide sequence starting from the 5′-terminus of chain A and proceeding to the 3′-terminus of chain A and then from the 5′-terminus of chain B to the 3′-terminus of chain B.

10.1021/bi012116t CCC: $22.00
Published on Web 04/02/2002

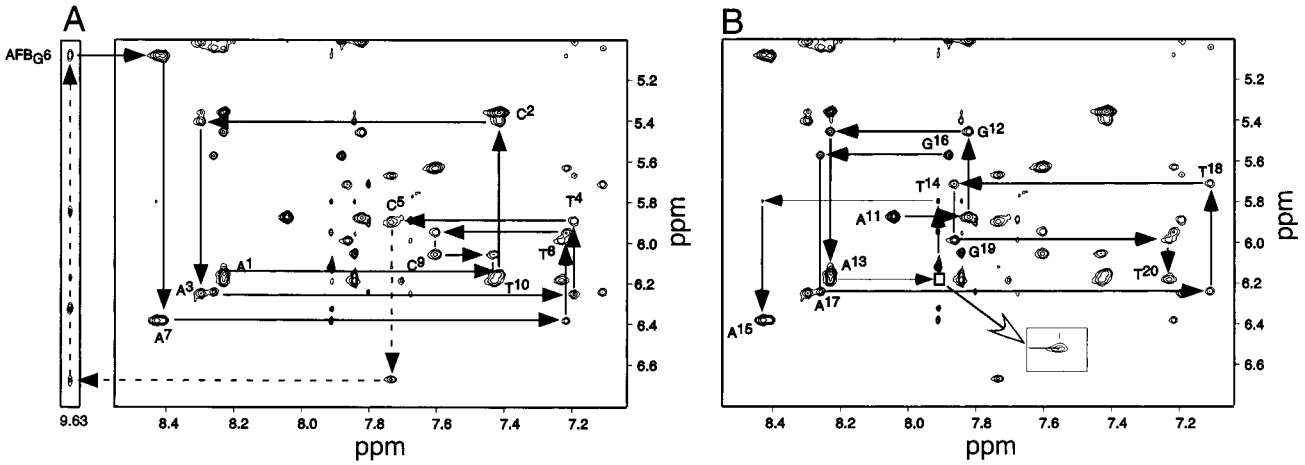

FIGURE 1: Expanded plots from the aromatic−anomeric region of the NOESY spectrum at 5 °C using a 200 ms mixing time, showing sequential NOE connectivities for (A) the modified strand and (B) the complementary strand. The resonances from $^{AFB}G^6$ were obtained in H_2O buffer. The A^{13} to T^{14} cross-peak is in the inset.

Scheme 1: Structure of the *trans*-8,9-Dihydro-8-(N7-guanyl)-9-hydroxy-aflatoxin B_1 Adduct and the Numbering Scheme for the Adducted Duplex d(ACATC^{AFB}GATCT)·d(AGATAGATGT) Containing the Mismatched $^{AFB}G^6$·A^{15} Pairing Interaction

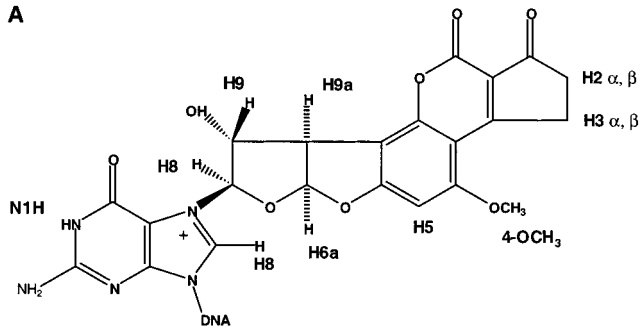

B 5′-A^1 C^2 A^3 T^4 C^5 $^{AFB}G^6$ A^7 T^8 C^9 T^{10}-3′
3′-$T^{20}$$G^{19}$$T^{18}$$A^{17}$$G^{16}$ $A^{15}$$T^{14}$$A^{13}$$G^{12}$$A^{11}$-5′

Oligodeoxynucleotide Numbering Scheme

trans-8,9-dihydro-8-(N7-guanyl)-9-hydroxy-aflatoxin B_1 adducts embedded in these two sequences have been refined from NMR data, providing a more quantitative view of the intercalated structures (*34*, *35*). In an additional refined solution structure of an AFB_1 adduct, an extra adenine was placed opposite the AFB_1 moiety. In this instance also, the aflatoxin moiety was intercalated above the 5′ face of the modified guanine (*36*). Intercalation thus appears to be a general feature of the *trans*-8,9-dihydro-8-(N7-guanyl)-9-hydroxy-aflatoxin B_1 adduct.

The availability of the aflatoxin epoxide (*20*) and site-specifically modified oligodeoxynucleotides enabled site-specific mutagenesis experiments to be conducted with the *trans*-8,9-dihydro-8-(N7-guanyl)-9-hydroxy-aflatoxin B_1 adduct. When site-specifically AFB_1-modified M13 bacteriophage were inserted into *Escherichia coli* and evaluated as to replication (*37*−*39*), the intercalated *trans*-8,9-dihydro-8-(N7-guanyl)-9-hydroxy-aflatoxin B_1 adduct induced G·C → T·A base pair substitutions (*30*, *31*), an observation which corroborated earlier observations from random mutagenesis (*3*, *4*). The site-specific methodology distinguished G·C → T·A transversions induced by the cationic lesion from those induced by depurination of the N7 adduct (*30*, *31*). The AFB_1-induced transversions were dependent on *mucAB* while those derived from the apurinic sites were dependent upon *umuDC*. This supported the contention that the *trans*-8,9-dihydro-8-(N7-guanyl)-9-hydroxy-aflatoxin B_1 lesion was responsible for G·C → T·A transversions. It was of particular interest that 13% of the AFB_1-induced mutations in vivo were C → T transitions targeted at the cytosine 5′ to the lesion site. The latter mutations suggested that AFB_1 also disturbed DNA replication 5′ to the lesion site and were correlated with structural data in which the cationic AFB_1 moiety intercalated on the 5′ side of the modified guanine.

The *trans*-8,9-dihydro-8-(N7-guanyl)-9-hydroxy-aflatoxin B_1 adduct blocked translesional DNA synthesis by DNA polymerase I (*exo*-) at the adducted site and one nucleotide 3′ to the adducted site (*40*). Correct incorporation of cytosine opposite the lesion led to blockage, while incorrect incorporation of adenine allowed full-length extension. The in vitro experiments using polymerase I yielded only base pair substitutions at the lesion site, not the substitutions at the 5′-neighbor base as were observed in vivo (*40*).

In light of site-specific mutagenesis experiments showing G → T transversions induced by the cationic AFB_1 adduct in the d(ATC^{AFB}GAT) sequence context and replication studies showing bypass of the adduct by polymerase I *exo*- but with misincorporation of dA, it was of interest to examine the structure of the d(ATC^{AFB}GAT) adduct when mispaired with dA. The G·A mismatch conformation is dependent on the environment and flanking base (*41*, *42*). NMR (*41*−*50*) and crystallographic (*51*−*53*) studies reported G_{anti}·A_{anti} (*46*), G_{syn}·A_{anti} (*48*, *51*), and G_{anti}·A_{syn} (*52*, *53*) conformations. A sheared G·A pairing exists for tandem G·A mismatches (*41*, *49*). The mismatch has also been examined in the context of PAH adduction at the exocyclic amino group of deoxyadenosine (*54*−*56*).

Presently, the structure of d(ACATC^{AFB}GATCT)·d(AGATAGATGT), which contains the ^{AFB}G·A mispairing interaction (Scheme 1), has been refined from NMR data. The results show that the characteristic 5′-intercalation of the aflatoxin moiety is maintained. The mismatched duplex exists in a single conformation at neutral pH. The mis-

matched dA is in the anti conformation about the glycosyl bond and is extruded toward the major groove. It does not participate in hydrogen bonding with ^{AFB}G. The mismatched structure is compared with the corresponding unmodified G·A mismatch and with the properly paired ^{AFB}G·C adduct (*35*). The correctly paired oligodeoxynucleotide exhibits Watson−Crick-type geometry at the ^{AFB}G·C pair and melts at higher temperature than does the mismatched ^{AFB}G·A duplex. The unmodified mismatched G·A duplex exhibits spectral line broadening at neutral pH and melts at a lower temperature than does the mismatched ^{AFB}G·A duplex. The observed differences suggest a structural basis for differential results of replication bypass experiments performed in vitro utilizing DNA polymerase I *exo*- that showed correct insertion of dC opposite ^{AFB}G blocks replication by the enzyme, whereas incorrect insertion of dA opposite ^{AFB}G allows full-length replication of the adducted template (*40*).

MATERIALS AND METHODS

Materials. AFB_1 was purchased from Sigma-Aldrich Chemicals, Inc. (St. Louis, MO). Unadducted oligodeoxynucleotides were purchased from Midland Certified Reagent Co. (Midland, TX). The oligodeoxynucleotides were desalted using Sephadex G-25 (Amersham Pharmacia, Inc., Piscataway, NJ).

Sample Preparation. Dimethyldioxirane was prepared (*57*) and reacted with AFB_1 to give AFB_1-*exo*-8,9-epoxide (*20*). *Caution*: *Crystalline aflatoxins are hazardous due to their electrostatic nature and should be handled using appropriate containment procedures and a respiratory mask to prevent inhalation. Aflatoxins can be destroyed by treatment with NaOCl. It should be assumed that aflatoxin* epoxides *are highly toxic and carcinogenic. Manipulations should be carried out in a well-ventilated hood with suitable containment procedures.* The oligodeoxynucleotide d(ACATC^{AFB}GATCT) was prepared by adding the epoxide dissolved in methylene choride to an aqueous solution containing d(ACATCGATCT) dissolved in 2 mM sodium phosphate (pH 7.5) at 5 °C in a dark room to form a two-phase mixture. Five equal aliquots of epoxide were added sequentially. The modified oligodeoxynucleotide was purified by HPLC using a C18 column (Hamilton, Inc., Reno, NV), equilibrated at room temperature, and eluted with a 45 min gradient from 1% to 30% v/v acetonitrile in 2 mM sodium phosphate (pH 7.5), with a flow rate of 1.5 mL/min. The adducted oligonucleotide was desalted with Sepahadex G-25 equilibrated with 0.1 mM sodium phosphate (pH 7.5). The adducted duplex d(ACATC^{AFB}GATCT)·d(AGATAGATGT) was prepared by titration of the complementary strand. The progress of the titration was monitored by the intensity of the aflatoxin H6a resonance observed by NMR at 6.63 ppm upon addition of the complementary strand. The integrity of the samples was examined by HPLC periodically since the cationic guanine N7 adduct slowly underwent depurination.

UV Melting. Experiments were carried out on a Cary 4E spectrophotometer (Varian Associates, Palo Alto, CA). The buffer was 10 mM sodium phosphate, 0.05 mM Na_2EDTA, and 1 M NaCl at pH 7.0. It was degassed. The concentrations were adjusted to 4.8×10^{-6} M in a 1 cm cuvette. The temperature was increased at a rate of 0.5 °C/min from 5 to 85 °C. Absorbance was measured at 260 nm. The melting temperatures of the native and modified oligodeoxynucleotides were calculated by determining the midpoints of the melting curves from the first-order derivatives.

NMR Spectroscopy. ^{1}H spectra were recorded at 800.23, 600.21, and 500.13 MHz. For observation of nonexchangeable protons, the sample was dissolved in 0.5 mL of 0.01 M sodium phosphate containing 0.1 M NaCl and 0.05 mM Na_2-EDTA at pD 7.4. The sample was dissolved in 99.96% D_2O. For observation of exchangeable protons, the sample was dissolved in 9:1 H_2O:D_2O. Most experiments were performed at 5 °C. Spectra of exchangeable protons were obtained at 0 °C. The temperature was controlled to ±0.5 °C. A phase-sensitive NOESY spectrum with 350 ms mixing time was used for assignment of nonexchangeable protons. The watergate pulse sequence suppressed the water signal (*58*). The phase-sensitive NOESY spectra used in the nonexchangeable proton resonance assignments were recorded at 5 °C using TPPI quadrature detection. Typical acquisition parameters were 1K real data points in the d_1 dimension with 32 acquisitions per FID, 2K real data points in the d_2 dimension, relaxation delay of 2 s, and a sweep width in both dimensions of 8 kHz. The data were processed using FELIX (version 97.0, Accelrys, Inc., San Diego, CA) on Silicon Graphics (Mountain View, CA) Octane workstations. The data in the t_1 dimension were zero-filled to give a matrix of 2K × 2K real points. A skewed sine-bell-square apodization function with a 90° phase shift was used in both dimensions. T_1 relaxation experiments were carried out with the $180°-\tau-90°$ sequence. Variable τ delays from 0.1 to 0.35 s were employed with 0.05 s increments. A total of 16 transients were recorded per cycle × 40 cycles for a total of 640 transients/FID. Chemical shifts were referenced internally to H_2O.

Starting Structures. A- (*59*) and B-DNA (*59*, *60*) were built with INSIGHTII (Accelyris, Inc., San Diego, CA). AFB_1 was intercalated above the 5′ face of G^6, and a covalent bond was created between AFB_1 C8 and G^6 N7. The adducted guanine N7 atom was assigned sp^2 hybridization. The electrostatic potential for the ^{AFB}G nucleotide was calculated using GAUSSIAN 98 (*61*) with the basis set 6-31G*. Partial charges were derived from electrostatic potentials using the RESP module of AMBER 6.0 (*62*). The partial charges (Supporting Information) were incorporated into subsequent PEM and rMD calculations. The A- and B-DNA structures were minimized by the conjugate gradient method for 200 iterations without experimental restraints to give the starting structures IniA and IniB for subsequent RMA and rMD calculations.

Distance Measurements. NOESY spectra measured at mixing times of 120, 150, and 200 ms were used for distance measurement. Footprint boxes were selected manually with FELIX to fit well-resolved peaks at a contour level which showed the weak NOEs but not the spectral noise. A larger error was assigned to the overlapped peaks. For each of the three mixing times, a hybrid intensity matrix was constructed using MARDIGRAS (*63*), which consisted of experimental intensities supplemented with calculated intensities from IniB. RMA using CORMA (*64*) yielded internuclear distances. Isotropic tumbling with t_c of 2−4 ns was assumed. The methyl jump model 3 accounted for the rapid spin of the methyl groups (*65*). Additional distance restraints were

determined from the NOESY spectrum measured in H_2O and from a NOESY spectrum measured in D_2O buffer using a 2.5 s delay. Larger error bounds were allowed for the latter distances since they were qualitatively classified as long, medium, and short range by visual inspection of the spectrum. Deoxyribose torsion angle restraints were derived from DQF-COSY data. Empirical base pairing distance and planarity restraints were included. Torsion angle restraints were used to prevent excessive propeller twisting of Watson−Crick base pairs.

Restrained Molecular Dynamics. Calculations with X-PLOR (*66*) were performed in vacuo without explicit counterions. The effective energy function was comprised of two terms describing distance and dihedral restraints, both of which were in the form of a standard square well potential (*67*). Bond lengths involving hydrogens were fixed with the SHAKE algorithm (*68*). The distance restraints were divided into categories. These were based on standard deviations obtained from MARDIGRAS. Force constants of 10 kcal mol^{-1} $Å^{-2}$ for empirical hydrogen bonding, 20 kcal mol^{-1} $Å^{-2}$ for torsion angle restraints, and 50, 45, 40, 35, and 30 kcal mol^{-1} $Å^{-2}$ for the five classes of NOE restraints were used. The calculations were coupled to a heating bath with a target temperature of 1000 K. The target temperature was reached in 5 ps and was maintained for 15 ps. The molecules were cooled to 300 K over 5 ps and maintained at that temperature for 25 ps of equilibrium dynamics. The force constants for the five classes of NOE restraints were scaled up for 3−5 ps during the heating period to 150, 130, 100, 100, and 100 kcal mol^{-1} $Å^{-2}$ in the order of confidence factor. These weights were maintained during the remainder of the heating period and for the first 5 ps of the equilibrium dynamics period. They were then scaled down to 50, 45, 40, 35, and 30 kcal mol^{-1} $Å^{-2}$ in the order of confidence factor. The torsion angle and base pair distance force constants were scaled up to 100 kcal mol^{-1} $Å^{-2}$ during the same period as for the NOE restraints. They were scaled back to 20 and 10 kcal mol^{-1} $Å^{-2}$, also at the same time as the NOE restraints. Backbone torsion angles were restrained during high-temperature dynamics. For base pairs A^1·C^{20}, C^2·G^{19}, A^3·T^{18}, T^4·A^{11}, A^7·T^{14}, T^8•A^{13}, C^9·G^{12}, and T^{10}·A^{11}, torsion angles were restricted to ranges that could sample both A- and B-DNA conformations. Force constants for the C^5·G^{16} and $^{AFB}G^6$·A^{15} torsion angles were half the magnitude of those used elsewhere. The coordinate sets were archived every 0.1 ps over the last 15 ps of the rMD simulation. The emergent structures were averaged and subjected to conjugate gradient energy minimization.

The emergent structure was solvated, and explicit counterions were added. In all, 17 Na^+ ions were added to neutralize the system using the Leap module in AMBER 6.0. The system was solvated with a rectangular box of TIP3P waters (*69*) extending ∼10 Å from the DNA atoms in three dimensions. A subsequent rMD calculation used the SANDER module of AMBER 6.0 (*70*) and the Cornell et al. force field (*71*), including the Parm94.dat parameter set. The Particle Mesh Ewald method (*72*, *73*) approximated nonbonded interactions. The NOE distance restraints were given a force constant of 20 kcal mol^{-1}. The suger pucker and torsion angle restraints were set to 2 kcal mol^{-1} rad^{-1}. The SHAKE algorithm constrained bonds involving protons to a tolerance of 0.0005 Å. A 1 fs time step was used. The rMD calculations were run for 1.4 ns, and coordinates were captured every 200 ps.

Convergence was evaluated using energy and energy-ordered rmsd profiles (*74*, *75*). Back-calculation of theoretical NMR intensities from the emergent structures was performed using CORMA (version 4.0) (*64*). The refined structures were analyzed using 3DNA (*76*). The helicoidal analysis was performed separately for the two fully base paired regions of the molecule, while parameters for the unpaired adenine were recorded manually using INSIGHTII for graphical display.

RESULTS

Thermal Stability. The stability of d(ACATC^{AFB}GATCT)·d(AGATGATGT) was examined by UV melting. It was compared with the corresponding unadducted sequence containing an A·G mismatch. The melting temperature of the adducted mismatched oligodeoxynucleotide was 35 °C. The cationic AFB_1 adduct increased the melting temperature of the A·G mismatch by 4 °C as compared to the unmodified A·G mismatched duplex. It was also compared with the duplex in which ^{AFB}G was correctly paired with dC, d(ACATC^{AFB}GATCT)·d(AGATCGATGT). In this case, a decrease in melting temperature of 10 °C was observed. Hence the introduction of the mismatch opposite to the lesion site resulted in a decreased melting temperature as compared to the correct pairing interaction. The differences in melting temperature provided estimates of T_m values for the helix−coil transition. This was not a reversible system. Upon melting of the duplex a small but measurable amount of depurination occurred. Because of the tendency toward depurination as the temperature was increased, most NMR data were collected at 5 °C. At this temperature, the cationic adduct was sufficiently stable over the time period required to collect two-dimensional NMR spectra.

NMR Spectroscopy. (a) DNA Proton Assignments. Nonexchangeable DNA protons were assigned using standard methods to identify sequential connectivities (*77*, *78*) (Figure 1). NOESY connectivities through the adducted strand were disrupted by the presence of the aflatoxin lesion. While the T^4 H1′ → C^5 H6 cross-peak was observed, no connectivity was observed between C^5 H1′ → $^{AFB}G^6$ H8 in D_2O. The resonance from $^{AFB}G^6$ H8 was observed in H_2O. The 9.63 ppm resonance assigned to $^{AFB}G^6$ H8 exhibited NOEs to the H6a proton of the aflatoxin moiety as well as the expected intranucleotide NOE to $^{AFB}G^6$ H1′. The latter resonance showed the expected NOE to A^7 H8 (Figure 1A). Likewise, C^5 H6 exhibited an NOE to H6a of the aflatoxin moiety, thus allowing the sequential connectivites to be traced from C^5 to A^7 in the modified strand. In the complementary strand, the sequential NOE between T^{14} H1′ → A^{15} H8 was weak, and A^{15} H1′ → G^{16} H8 at the site across from the lesion was missing. Except for the site of the ^{AFB}G·A mismatch and T^{14}, the internucleotide connectivities were characteristic of B-type DNA. The NOESY connectivities through the adducted strand were disrupted by the presence of the aflatoxin lesion similar to that reported before (*36*). The adenine H2 protons were assigned on the basis of NOEs with their own H1′ protons and the NOEs to the H1′ proton of the nucleoside on the 3′ side and confirmed by using a nonselective inversion recovery experiment. The assignment of A^{15} H2

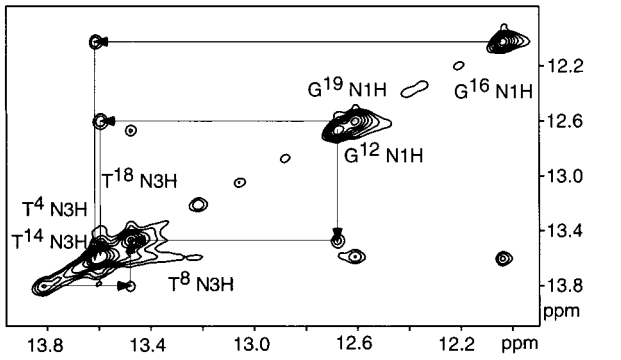

FIGURE 2: Expanded plot showing sequential NOE connectivities for the imino protons of base pairs $C^2 \cdot G^{19} \rightarrow C^5 \cdot G^{16}$ and $A^7 \cdot T^{14} \rightarrow C^9 \cdot G^{12}$. The labels represent the imino proton of the designated base. The NOESY spectrum was collected at 200 ms mixing time and 0 °C.

was problematic in that it resonated at the same frequency as T^{14} H6 (Figure 8). This represented a 0.85 ppm downfield shift of T^{14} H6 as compared to its resonance position in the unmodified duplex. Its line width was narrow, and its NOE cross-peaks were small. T^{14} H2′ and H2″ were shifted upfield (δ 1.29 and 1.67 ppm, respectively) compared to the corresponding resonances in the unmodified mismatched duplex (δ 2.56, 2.82 ppm). The cross-peak between T^{14} H6 and H1′ was weak in spectra of both the modified and unmodified mismatched duplexes. The assignments of the DNA proton resonances are tabulated in Table S1 in the Supporting Information.

(b) Exchangeable Protons. The imino resonance $^{AFB}G^6$ N1H was not identified, probably due to broadening associated with the cationic charge introduced into the purine ring by alkylation at guanine N7. The assignments of the remaining Watson−Crick base-paired imino protons were based upon sequential connectivities between the imino protons of adjacent base pairs (Figure 2) and to base-paired amino protons (*79*). Sequential assignments of the imino protons from base pairs $C^2 \cdot G^{19} \rightarrow C^5 \cdot G^{16}$ and $A^7 \cdot T^{14} \rightarrow C^9 \cdot G^{12}$ were obtained unequivocally. No NOE connectivities were observed between G^{16} N1H and A^{15} H2. The T^4 N3H and T^{18} N3H resonances exhibited similar chemical shifts. The imino proton of T^{14} was assigned on the basis of its cross-peak with A^7 H2 and cross-peak with T^8 imino protons. These assignments are listed in Table S2 of the Supporting Information.

(c) Aflatoxin Proton Assignments. Figure 3 shows the portion of the NOESY spectrum that displays the aflatoxin spin systems. The connectivities between the AFB_1 H6a, H8, H9, and H9a furanose protons located these resonances at δ 6.63, 6.3, 6.07, and 3.87 ppm, respectively, whereas the NOE between AFB_1 H5 and AFB_1 $-OCH_3$ located these resonances at δ 5.51 and 3.43 ppm, respectively. Only one set of resonances corresponding to AFB_1 protons was observed. This indicated the presence of a single conformational species at the adducted mismatched base pair. The methylene protons on the cyclopentenone ring were partially superimposed with the deoxyribose H2′, H2″ protons as well as the thymine CH_3 protons. The assignments (Figure 4) were consistent with expected chemical shift differences between the H3 α,β and H2 α,β resonances. They were also consistent with assignments from previous AFB_1-adducted samples (*32*), NOE intensity patterns of among the four methylene protons,

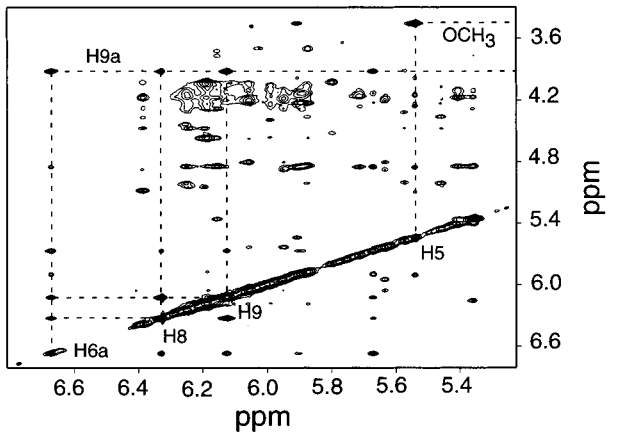

FIGURE 3: Expanded NOESY spectrum at 250 ms mixing time showing the assignments for the protons from AFB_1 furanose ring. The experiment was at 5 °C.

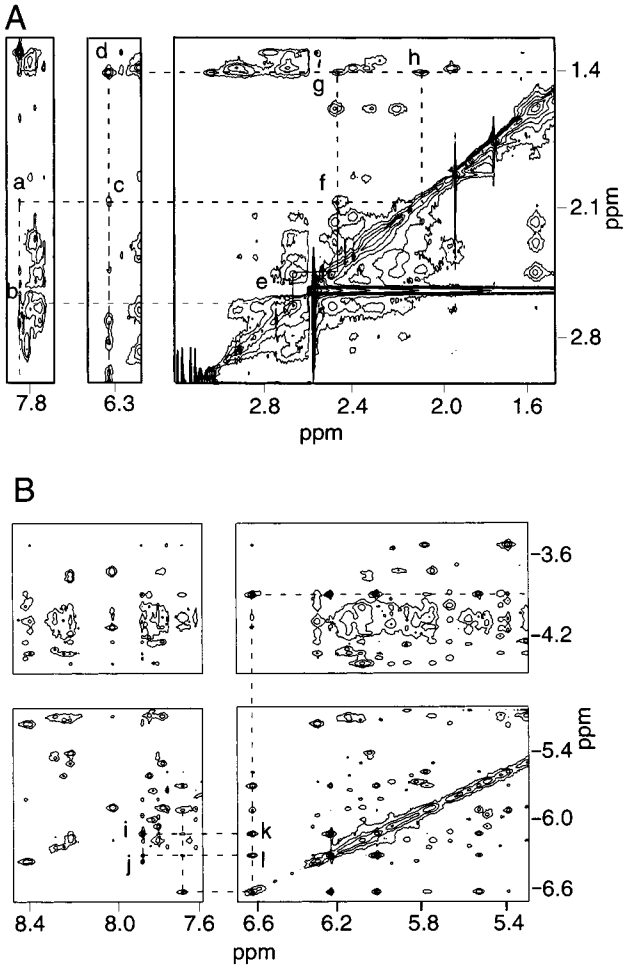

FIGURE 4: Tile plot showing NOE cross-peaks between nonexchangeable protons of DNA and AFB_1 protons. (A) NOE connectivities between A^{15} H2, H1′ and AFB_1 methylene protons: a−h, A^{15} H2 → $AFB_1 2\beta$, A^{15} H2 → $AFB_1 3\beta$, A^{15} H1′ → $AFB_1 2\beta$, A^{15} H1′ → $AFB_1 2\alpha$, $AFB_1 3\beta$ → $AFB_1 3\alpha$, $AFB_1 3\alpha$ → $AFB_1 2\beta$, $AFB_1 2\alpha$ → $AFB_1 3\alpha$, and $AFB_1 2\beta$ → $AFB_1 2\alpha$. (B) NOE connectivities between A^{15} H2, H1′ and AFB_1 furanose protons: i−l, A^{15} H2 → $AFB_1 8A$, A^{15} H2 → $AFB_1 9$, $AFB_1 6A$ → $AFB_1 9$, and AFB_1-6A → $AFB_1 8A$.

and specific AFB_1−DNA NOEs to either the 5′-face H2 and H3 α protons or the 3′-face H2 and H3 β protons. Stronger cross-peaks were observed between the diastereotopic geminal protons at each position; weaker NOEs were observed

Table 1: NOEs Observed between the AFB_1 Adduct and DNA

AFB_1 proton	DNA protons					
H5	C^5 H2′	C^5 H2″	C^5 H1′	$^{AFB}G^6$ H1′	C^5 H6	$^{AFB}G^6$ H8[a]
H6a	C^5 H5	C^5 H2″	C^5 H2′	$^{AFB}G^6$ H8[a]	C^5 H6	T^4 H1′
H8	$^{AFB}G^6$ H8[a]	C^5 H6	A^{15} H2			
H9	$^{AFB}G^6$ H8[a]	A^{15} H2				
H9a	C^5 H2′	C^5 H1′	C^5 H6	$^{AFB}G^6$ H8[a]		
4-OCH_3	C^5 H4′	C^5 H2″	$^{AFB}G^6$ H1′	C^5 H1′	C^5 H2′	$^{AFB}G^6$ H4′
			$^{AFB}G^6$ H8[a]	G^{16} H1		
$H2_\alpha$	A^{15} H1′	A^{15} H2	G^{16} H5″	G^{16} H4′		
$H2_\beta$	A^{15} H1′	A^{15} H2				
$H3_\beta$	A^{15} H2					
$H3_\alpha$	G^{16} H1′	G^{16} H1				

[a] NOE was observed in H_2O.

between the vicinally coupled protons at each position. The assignments of the AFB_1 ^1H resonances are listed in Table S3 of the Supporting Information.

(d) NOEs between Aflatoxin and DNA Protons. A total of 38 NOEs were observed between aflatoxin and DNA protons; 12 of these were cross-strand NOEs (Table 1). AFB_1 H8 and H9 exhibited long-range, cross-strand NOEs to A^{15} H2 (Figure 4). Similar long-range NOEs were also observed between the AFB_1 H2b proton and A^{15} H2 and A^{15} H1′ protons (Figure 4). These observations confirmed that A^{15} was in the anti conformation about the glycosyl bond. AFB_1 H6a and H9a, the two protons located at the juncture of the fused furan rings, showed a number of NOEs in the 5′ direction. AFB_1 H6a showed NOEs to C^5 H5, C^5 H6, C^5 H2′, and C^5 H2″ of the C^5•G^{16} base pair. AFB_1 H9a showed NOEs to C^5 H1′, C^5 H2′, and C^5 H6. The AFB_1 H5 proton showed NOEs to C^5 H2′, C^5 H2″, C^5 H1′, and C^5 H6. The AFB_1 −OCH_3 protons, located on the coumarin ring, showed NOEs to C^5 H1′, C^5 H4′, C^5 H2′, C^5 H2″, $^{AFB}G^6$ H1′, $^{AFB}G^6$ H8, A^{15} H2, and G^{16} H1′. The NOEs between the AFB_1 protons and the flanking bases 5′ to the lesion site suggested that the aflatoxin moiety intercalated on the 5′ face of the modified guanine.

(e) Unmodified Mismatched Duplex. The exchangeable and nonexchangeable protons were assigned, and the NOE connectivity was as expected for a right-handed B-like duplex, except for the mismatch site. At pH 7 the A^{15} H8−H1′ cross-peak was broad, suggesting the presence of multiple conformations at the mispairing site, in intermediate exchange on the NMR time scale. The T^{14} H6 and A^{15} H8 aromatic protons were shifted upfield. The G^6 imino proton resonance was sharp. It shifted upfield to 11.5 ppm and exhibited a cross-peak to the A^{15} H2 proton (Figure S2 in the Supporting Information).

Structural Refinement. There were 329 experimental distance restraints derived from nonexchangeable ^1H NOEs by MARDIGRAS. These consisted of 181 intranucleotide restraints, 110 internucleotide restraints, and 38 adduct−DNA restraints (Table 2). The restraints were approximately evenly distributed along the length of the oligodeoxynucleotide, except for T^{14} and A^{15}. The DQF-COSY data for bases except $^{AFB}G^6$, A^{15}, and T^{14} were consistent with the C2′-endo sugar conformation. Therefore, except $^{AFB}G^6$, A^{15}, and T^{14}, the deoxyribose rings were restrained to the C2′-endo conformation (*80*). The observation that there were no unusually shifted ^{31}P resonances indicated that the backbone geometry was similar to that for B-DNA (*81*). Empirical hydrogen-bonding restraints between base pairs were used except for the $^{AFB}G^6$•A^{15} mismatched base pair. The restraints used for rMD calculations are listed in Table S4 of the Supporting Information.

Table 2: Analysis of the rMD-Generated Structures of the AFB_1 Adduct in the Mismatched ^{AFB}G•A Pair

NMR restraints	
total no. of distance restraints	329
interresidue distance restraints	181
intraresidue distance restraints	110
DNA−AFB_1 distance restraints	38
deoxyribose pseudorotation restraints	15
backbone torsion angle restraints	93
hydrogen-bonding restraints	33
rms deviations from ideal geometry[a]	
rmsd of NOE violations (Å)	0.05 ± 0.001
no. of NOE violations >0.2 Å in entire duplex	8 ± 2
improper angle (deg)	0.33 ± 0.03
pairwise rmsd (Å) over all atoms[a]	
⟨rMDA⟩ vs ⟨rMDB⟩	1.05 ± 0.15

[a] ⟨rMDA⟩, average of 10 converged structures starting from A-DNA; ⟨rMDB⟩, average of 10 converged structures from B-DNA.

Calculations begun from IniA and IniB structures generated by INSIGHTII yielded 10 "converged" structures (Figure 5). The maximum pairwise rmsd for the converged structures was 0.55 Å, indicating a well-defined conformation. A further 1.4 ns rMD simulation in the presence of solvent and counterions was performed using the AMBER force field. The maximum pairwise rmsd for the structures emergent from the AMBER calculations was 1.2 Å. Sixth root residual factors R_1^x calculated from complete relaxation matrix analysis using CORMA (*64*) are collected in Table 3. The starting structure IniA did not provide a satisfactory fit for the CORMA calculations. The IniB starting structure provided a better fit, suggesting that the actual conformation of the adducted duplex was closer to B-form DNA than to A-form DNA. Nevertheless, the R_1^x values arising from comparison of the IniB structure with the experimental NOEs were greater than 15%, suggesting that the AFB_1 adduct perturbed the duplex structure at the lesion site. The refined structure gave R_1^x values in the range of 10.5−11.6% as a function of NOE mixing time, with the best agreement shown to the 150 ms mixing time NOE data. Overall, the relaxation matrix calculations suggested that the refined structures provided reasonable models for the adducted duplex.

Structural Evaluation. The refined structure was a right-handed duplex (Figure 6). Figures 7 and 8 show detailed views of the adduct site. The duplex suffered localized distortion at and immediately adjacent to the adduct site, evidenced by the increased rise of 7.7 Å as compared to the

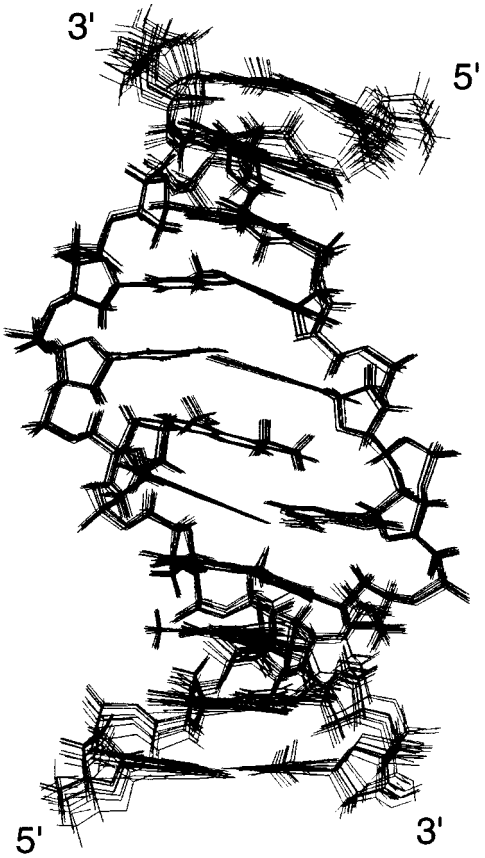

FIGURE 5: Superposition of 10 structures emergent from rMD calculations of the AFB_1-modified mismatched duplex. The large number of NOEs observed between the AFB_1 moiety and the DNA resulted in excellent convergence of the calculations at and adjacent to the lesion site.

Table 3: Sixth Root Residual Indices R_1^x as a Function of NOE Mixing Time[a,b]

structure	120 ms	150 ms	200 ms
rMD final[c]	11.6	10.5	10.9
rMDB[d]	11.9	10.8	11.7
IniB[e]	16.5	15.1	19.6

[a] All values for R_1^x are $\times 10^{-2}$. To exclude end effects, only the eight inner base pairs were included in calculations. [b] $R_1^x = \sum|(a_o)_i^{1/6} - (a_c)_i^{1/6}|/\sum|(a_o)_i^{1/6}|$, where (a_o) and (a_c) are the intensities of observed (nonzero) and calculated NOE cross-peaks. [c] Calculated for the structure emergent from rMD calculations in the presence of counterions and solvent. [d] Calculated for the structure emergent from rMD calculations in vacuo. [e] Calculated from the B-form starting structure.

value of 3.5 Å normally observed for B-DNA between mismatch $^{AFB}G^6 \cdot A^{15}$ and $C^5 \cdot G^{16}$. These two base pairs buckled in opposite directions away from the intercalated aflatoxin moiety. Changes of 24° and −14° in buckle were calculated for $C^5 \cdot G^{16}$ and $^{AFB}G^6 \cdot A^{15}$, respectively, similar to what was observed in crystallographically determined intercalation structures (*82*, *83*). Unwinding of the duplex was observed. The helical twist at the intercalation site $C^5 \cdot G^{16} \rightarrow {}^{AFB}G^6 \cdot A^{15}$ was reduced to ~8.1°, as compared to the expectation value of ~34°. This was also evident from the 55° base pair opening value for the mismatched $^{AFB}G^6 \cdot A^{15}$ pair. The rMD calculations predicted that A^{15} was not hydrogen bonded to $^{AFB}G^6$ but rather was shifted toward the major groove. Helicoidal analysis showed that with the exception of base pair step 5, $C^5 \cdot G^{16} \rightarrow {}^{AFB}G^6 \cdot A^{15}$, interbase pair parameters converged to values consistent with a right-handed B-like helix. Larger deviations were found for base pair shearing, stretch, rise, propeller twist, and opening near and at the adduct site. The helicoidal analysis is detailed in Figure S3 of the Supporting Information.

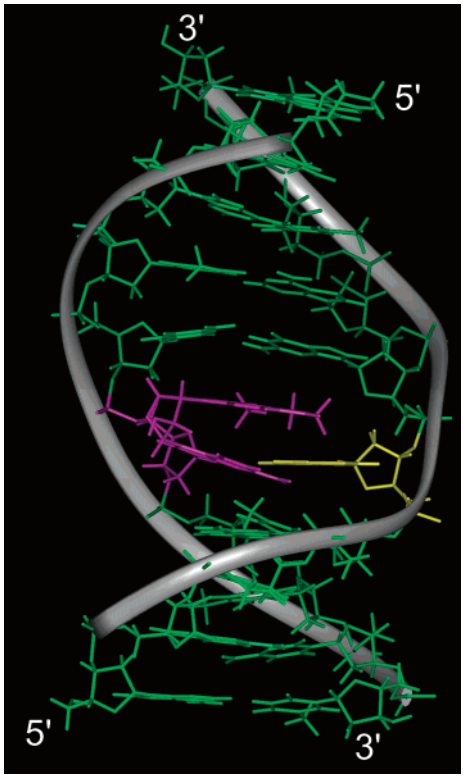

FIGURE 6: Stick and ribbon model showing the average structure of the mismatched AFB_1-modified duplex predicted from rMD calculations. The modified nucleotide $^{AFB}G^6$ is shown in magenta. The mismatched A^{15} is shown in yellow. One consequence of AFB_1 intercalation 5′ to the modified deoxyguanosine was the increased rise and unwinding of the duplex at the lesion site.

DISCUSSION

In DNA, mismatches arise through errors in replication or through recombination processes. If not repaired, they lead to mutations in the genome. Thus, their recognition and the efficiency of their repair are of considerable interest. The G → T transversion is the predominant mutation introduced by aflatoxin B_1 (*3*, *30*). Presumably, this mutation occurs as a consequence of the incorrect incorporation of dATP opposite the ^{AFB}G lesion during DNA replication. Site-specific mutagenesis data carried out in a bacterial system supported the notion that the *trans*-8,9-dihydro-8-(N7-guanyl)-9-hydroxy-aflatoxin B_1 lesion was responsible for G·C → T·A transversions (*31*). The observation that the *trans*-8,9-dihydro-8-(N7-guanyl)-9-hydroxy-aflatoxin B_1 adduct allowed correct incorporation of cytosine by DNA polymerase I (*exo*-) opposite but resulted in polymerase blockage, while incorrect incorporation of adenine allowed full-length extension (*40*), led to further interest in the structure of the adduct mismatched with deoxyadenosine.

The $^{AFB}G \cdot A$ Mismatched Oligodeoxynucleotide. In the mismatched oligodeoxynucleotide, the aflatoxin moiety intercalated above the 5′ face of the modified guanine, such that the aflatoxin methoxy and cyclopentenone ring protons faced into the minor groove, whereas the furofuran ring protons faced into the major groove (Figure 7). The overall

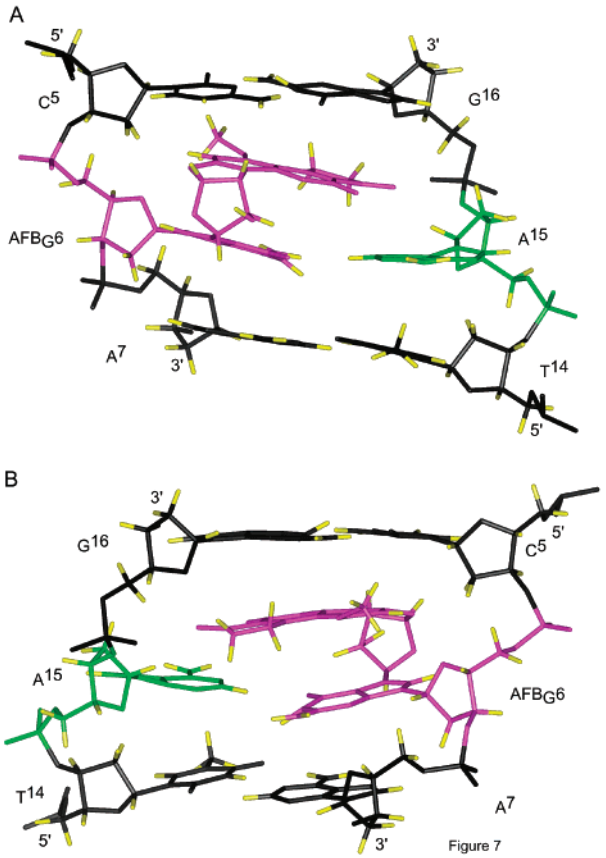

FIGURE 7: Detailed view of the mispaired $^{AFB}G^6 \cdot A^{15}$ site and the flanking base pairs $C^5 \cdot G^{16}$ and $A^7 \cdot T^{14}$. The adducted nucleotide $^{AFB}G^6$ is shown in magenta. The mismatched A^{15} is shown in green. Protons are shown in yellow. (A) View from the major groove. The AFB_1 H6a, H8, H9, and H9a protons face the major groove. (B) View from the minor groove. The AFB_1 $-OCH_3$ and H5 protons face the minor groove, as do the AFB_1 methylene protons H2 α,β and H3 α,β.

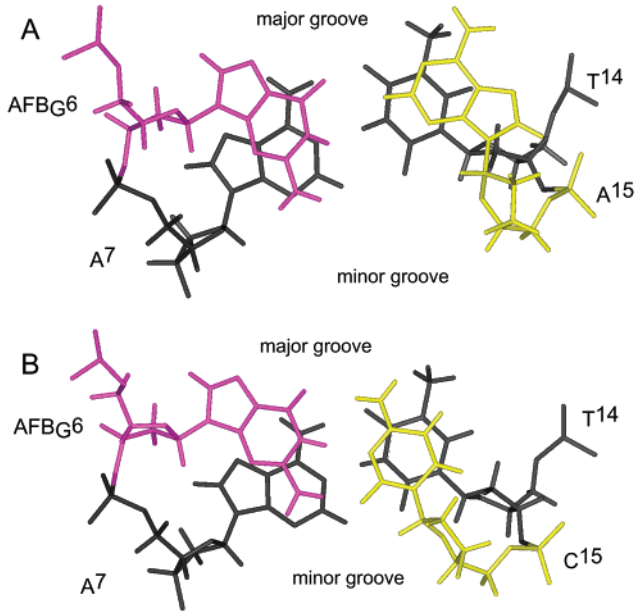

FIGURE 8: Comparison of the mismatched $^{AFB}G \cdot A$ structure with the correctly paired $^{AFB}G \cdot C$ structure (*35*). Stacking of the adducted base pair and the 3′ flanking bases as predicted from rMD calculations. The adducted nucleotide $^{AFB}G^6$ is shown in magenta. The 3′-neighbor base pair $A^7 \cdot T^{14}$ is shown in black. (A) Mismatched $^{AFB}G \cdot A$ structure. The mismatched nucleotide A^{15} is shown in yellow and is shifted toward the major groove. (B) Correctly paired $^{AFB}G \cdot C$ structure. The correctly paired C^{15} is shown in yellow.

conformation of the DNA remained right-handed, and the principal perturbation to the DNA structure occurred at the site of the mismatched $^{AFB}G^6 \cdot A^{15}$ base pair. The intercalation of the AFB_1 moiety on the 5′ side of the adducted dG was reminiscent of other aflatoxin-adducted oligodeoxynucleotides (*32*, *34*, *36*). The AFB_1 protons had nearly identical chemical shifts and also exhibited the same pattern of NOEs to the 5′-flanking base in all cases. This motif appears to be a characteristic of the *trans*-8,9-dihydro-8-(N7-guanyl)-9-hydroxy-aflatoxin B_1 adduct which is conserved irrespective of the nature of the base complementary to the adducted dG.

The refined structure was supported by NOE evidence. The NOESY connectivities through the adducted strand were disrupted by the presence of the aflatoxin lesion similar to that reported before (*36*). A number of characteristic NOEs were observed between the aflatoxin moiety and the 5′-neighbor base pair, $C^5 \cdot G^{16}$. The aflatoxin H6a and H9a protons, facing the major groove, exhibited NOEs to C^5 H5. AFB_1 H6a also showed an NOE to C^5 H6. The observations of NOEs between the AFB_1 4-OCH_3 and H5 protons to C^5 H1′ and $^{AFB}G^6$ H1′, and the NOE between the 4-OCH_3 protons and $^{AFB}G^6$ H4′, were consistent with intercalation. These oligodeoxynucleotide protons faced into the minor groove and suggested that the AFB_1 moiety spanned the helix. The presence of the AFB_1 moiety resulted in upfield chemical shifts for the protons of the AFB_1 moiety as compared to unbound aflatoxin. The pattern and magnitude of these chemical shift changes were supportive of the notion that the orientation of the covalently bound aflatoxin moiety was similar to previously observed structures (*36*).

The observations that the intensity of the A^{15} H8 to A^{15} H1′ cross-peak was smaller than cytosine H5−H6 cross-peaks and that A^{15} H2 exhibited a typical value for its chemical shift of 7.88 ppm supported the conclusion that the mismatched A^{15} was in the anti conformation about the glyosyl bond. This conclusion was also consistent with the observed NOEs from the A^{15} H2 proton to the aflatoxin protons. The cross-peak between A^{15} H2 and G^{16} H1′ also confirmed the glycosyl conformation of the mismatched adenine A^{15}. These would not have been consistent with the syn conformation.

The conclusion that A^{15} was not hydrogen bonded to $^{AFB}G^6$ but rather was shifted toward the major groove (Figure 8) was consistent with the observation that the $^{AFB}G^6$ N1H proton was not observed. The delocalization of the positive charge induced by alkylation of the guanine N7 position through the adducted base and aflatoxin moiety (*36*) was anticipated to cause broadening of the $^{AFB}G^6$ N1H proton. The downfield shift of $^{AFB}G^6$ H8 (Figure 1) was due to the positive charge on the imidazole ring of the modified guanine, which also increased the rate of exchange with solvent, rendering this proton resonance unobservable in the deuterated buffer. However, the ^{AFB}G N1H proton was observed in the correctly paired $^{AFB}G \cdot C$ adduct as a broadened signal shifted downfield in the spectrum (*24*). Thus, the failure to observe the $^{AFB}G^6$ N1H proton in the $^{AFB}G^6 \cdot A^{15}$ pairing interaction was consistent with the notion that it did not participate in hydrogen bonding and was exchange broadened. Further support for the predicted conformation in which A^{15} was shifted toward the major

groove was provided by rMD calculations in which specific potential base pairing restraints were incorporated between $^{AFB}G^{6}$ and A^{15}. In each instance, rMD calculations carried out with such restraints resulted in significant NOE violations when compared with the spectroscopic data. Additional evidence in support of the calculated structure involving A^{15} accrued from chemical shift perturbations at base pair A^{7}·T^{14}. That normal base pairing was present at A^{7}·T^{14} was evident from the cross-peaks between T^{14} N3H with T^{8} N3H and A^{7} H2, respectively.

Comparison to the Properly Paired ^{AFB}G·C Duplex. The conformation of the mismatched dA in the ^{AFB}G·A mismatched duplex was different as compared to dC in the correctly paired ^{AFB}G·C modified duplex (Figure 8) (*35*). Misincorporation of adenine opposite $^{AFB}G^{6}$ resulted in greater unwinding of the helix compared to the ^{AFB}G·C context. For ^{AFB}G·C, both the lesion site and 3′-flanking pair were in a position to base pair. The presence of base pairing was suggested by the observance of the ^{AFB}G N1H resonance, which underwent sufficiently slow exchange with solvent to be observable. This was predicted by the rMD calculations of the two helices. For the ^{AFB}G·C helix, the top view suggested that C^{15} is nicely stacked above T^{14}. In contrast, for the ^{AFB}G·A context (Figure 8), the calculations predicted A^{15} shifted toward the major groove, in an orientation in which it could not participate in hydrogen bonding with $^{AFB}G^{6}$. For the ^{AFB}G·A context the mismatched adenine was more stacked on the deoxyribose of T^{14} than above the nucleobase of T^{14}. This perhaps explained the unusual chemical shift effects observed for T^{14}. This orientation of the dA base in the ^{AFB}G·A duplex, moved away from the cationic adduct compared to ^{AFB}G·C, might provide a rationale for the observation that when dA was incorrectly inserted opposite ^{AFB}G, DNA polymerase I *exo*- successfully bypassed the adduct and continued replication (*40*).

Effect of the Aflatoxin B_1 Adduct on the G·A Mismatch. The results suggested AFB_1 stabilized a single conformation of the $^{AFB}G^{6}$·A^{15} base pair at neutral pH. The observed pattern of NOEs led to the conclusion that the glycosyl bond of A^{15} remained in the anti conformation. The corresponding duplex containing G^{6}·A^{15}, but lacking the AFB_1 adduct, exhibited spectral line broadening at neutral pH. This was interpreted to result from intermediate conformational exchange, possibly similar to that reported by Patel and co-workers (*48*). The possibility of sheared base pairing associated with tandem G·A mismatches (*41*, *49*) was ruled out. Sheared pairing was not expected because the $^{AFB}G^{6}$·A^{15} mismatch was incorporated into a nontandem sequence context. The absence of downfield ^{31}P shifts in the present instance was consistent with this conclusion (*42*, *44*). The results provide additional insight into the structure of a G·A mismatch in the presence of a DNA lesion. The ^{AFB}G·A mismatch structure differed from G·A mismatches in the presence of the adenyl N^{6} PAH adducts (*48*, *54*, *55*). The G·A mismatch pair was stable in the presence of a 10*S* adduct derived from addition of the dA N^{6} amino group to (+)-(7*R*,8*S*,9*S*,10*R*)-7,8-dihydroxy-9,10-epoxy-7,8,9,10-tetrahydrobenzo[*a*]pyrene. Two conformations of the mismatch in the presence of the PAH lesion were attributed to interconversion of the modified dA nucleotide between the syn and anti conformations about the glycosyl bond. In the major conformation, the glycosyl bond of the modified dA was in the syn conformation, resulting in the projection of the modified dA more into the major groove (*54*−*56*). The G·A mismatch pair was also examined in the presence of a 10*R* adduct derived from addition of the dA N^{6} amino group to (−)-(7*S*,8*R*,9*R*,10*S*)-7,8-dihydroxy-9,10-epoxy-7,8,9,10-tetrahydrobenzo[*a*]pyrene. The mismatched dA remained in the anti conformation about the glycosyl bond, with the dG being pushed into the major groove (*54*).

Biological Significance. Experiments using DNA polymerase I *exo*- in vitro showed that replication was blocked following correct insertion of dC opposite ^{AFB}G, but successful bypass occurred following incorrect incorporation of dA (*40*). The unmodified mismatched duplex appeared to be in a disordered state consisting of a blend of conformations. In contrast, the mispaired dA in the modified ^{AFB}G·A mismatch existed in a single conformation. The glycosyl bond of the mismatched dA was in the anti conformation. This was consistent with the observation that the oligodeoxynucleotide containing the ^{AFB}G·A mismatch had a lower melting temperature than did the oligodeoxynucleotide containing the correct ^{AFB}G·C pair. Our working hypothesis posits that the different structure of the ^{AFB}G·A mismatch pair as compared to the proper ^{AFB}G·C pair perhaps facilitates replication bypass of the AFB_1 lesion by DNA polymerase I *exo*- (*40*) following adventitious misincorporation of dA opposite the lesion.

ACKNOWLEDGMENT

We thank Dr. Zhijun Li for assistance with rMD calculations and Mr. Markus Voehler for assistance with NMR spectroscopy.

SUPPORTING INFORMATION AVAILABLE

Tables S1−S3, which detail the ^{1}H NMR chemical shift assignments, and S4, which shows the experimental distances and classes of restraints; Figures S1, which shows atomic names and types used in AMBER calculations for AFB_1 and the partial charges, S2, which shows the expanded sequential NOE connectivities for the unmodified G·A mismatched duplex, and S3, which shows helicoidal analysis of the refined structure.

REFERENCES

1. Busby, W. F., Jr., and Wogan, G. N. (1984) in *Chemical Carcinogens* (Searle, C. E., Ed.) pp 945−1136, American Chemical Society, Washington, DC.
2. McCann, J., Spingarn, N. E., Koburi, J., and Ames, B. N. (1975) *Proc. Natl. Acad. Sci. U.S.A. 72*, 979−983.
3. Foster, P. L., Eisenstadt, E., and Miller, J. H. (1983) *Proc. Natl. Acad. Sci. U.S.A. 80*, 2695−2698.
4. Foster, P. L., Groopman, J. D., and Eisenstadt, E. (1988) *J. Bacteriol. 170*, 3415−3420.
5. Bailey, G. S., Loveland, P. M., Pereira, C., Pierce, D., Hendricks, J. D., and Groopman, J. D. (1994) *Mutat. Res. 313*, 25−38.
6. Bailey, G. S., Williams, D. E., Wilcox, J. S., Loveland, P. M., Coulombe, R. A., and Hendricks, J. D. (1988) *Carcinogenesis 9*, 1919−1926.
7. McMahon, G., Davis, E. F., Huber, L. J., Kim, Y., and Wogan, G. N. (1990) *Proc. Natl. Acad. Sci. U.S.A. 87*, 1104−1108.
8. Soman, N. R., and Wogan, G. N. (1993) *Proc. Natl. Acad. Sci. U.S.A. 90*, 2045−2049.
9. Bressac, B., Kew, M., Wands, J., and Ozturk, M. (1991) *Nature 350*, 429−431.

10. Hsu, I. C., Metcalf, R. A., Sun, T., Welsh, J. A., Wang, N. J., and Harris, C. C. (1991) *Nature 350*, 427−428.
11. Greenblatt, M. S., Bennett, W. P., Hollstein, M., and Harris, C. C. (1994) *Cancer Res. 54*, 4855−4878.
12. Shen, H. M., and Ong, C. N. (1996) *Mutat. Res. 366*, 23−44.
13. Soini, Y., Chia, S. C., Bennett, W. P., Groopman, J. D., Wang, J. S., DeBenedetti, V. M., Cawley, H., Welsh, J. A., Hansen, C., Bergasa, N. V., Jones, E. A., DiBisceglie, A. M., Trivers, G. E., Sandoval, C. A., Calderon, I. E., Munoz Espinosa, L. E., and Harris, C. C. (1996) *Carcinogenesis 17*, 1007−1012.
14. Lunn, R. M., Zhang, Y. J., Wang, L. Y., Chen, C. J., Lee, P. H., Lee, C. S., Tsai, W. Y., and Santella, R. M. (1997) *Cancer Res. 57*, 3471−3477.
15. Mace, K., Aguilar, F., Wang, J. S., Vautravers, P., Gomez-Lechon, M., Gonzalez, F. J., Groopman, J., Harris, C. C., and Pfeifer, A. M. (1997) *Carcinogenesis 18*, 1291−1297.
16. Santella, R. M., Zhang, Y. J., Chen, C. J., Hsieh, L. L., Lee, C. S., Haghighi, B., Yang, G. Y., Wang, L. W., and Feitelson, M. (1993) *Environ. Health Perspect. 99*, 199−202.
17. Chen, C. J., Yu, M. W., Liaw, Y. F., Wang, L. W., Chiamprasert, S., Matin, F., Hirvonen, A., Bell, D. A., and Santella, R. M. (1996) *Am. J. Hum. Genet. 59*, 128−134.
18. Yu, M. W., Lien, J. P., Chiu, Y. H., Santella, R. M., Liaw, Y. F., and Chen, C. J. (1997) *J. Hepatol. 27*, 320−330.
19. Ueng, Y. F., Shimada, T., Yamazaki, H., and Guengerich, F. P. (1995) *Chem. Res. Toxicol. 8*, 218−225.
20. Baertschi, S. W., Raney, K. D., Stone, M. P., and Harris, T. M. (1988) *J. Am. Chem. Soc. 110*, 7929−7931.
21. Johnson, W. W., Harris, T. M., and Guengerich, F. P. (1996) *J. Am. Chem. Soc. 118*, 8213−8220.
22. Essigmann, J. M., Croy, R. G., Nadzan, A. M., Busby, W. F., Jr., Reinhold, V. N., Buchi, G., and Wogan, G. N. (1977) *Proc. Natl. Acad. Sci. U.S.A. 74*, 1870−1874.
23. Stone, M. P., Gopalakrishnan, S., Harris, T. M., and Graves, D. E. (1988) *J. Biomol. Struct. Dyn. 5*, 1025−1041.
24. Gopalakrishnan, S., Stone, M. P., and Harris, T. M. (1989) *J. Am. Chem. Soc. 111*, 7232−7239.
25. Gopalakrishnan, S., Byrd, S., Stone, M. P., and Harris, T. M. (1989) *Biochemistry 28*, 726−734.
26. Stone, M. P., Gopalakrishnan, S., Raney, K. D., Raney, V. M., Byrd, S., and Harris, T. M. (1990) in *Molecular Basis of Specificity in Nucleic Acid-Drug Interactions* (Pullman, B., and Jortner, J., Eds.) pp 451−480, Kluwer Academic Publishers, Dordrecht, The Netherlands.
27. Raney, K. D., Gopalakrishnan, S., Byrd, S., Stone, M. P., and Harris, T. M. (1990) *Chem. Res. Toxicol. 3*, 254−261.
28. Raney, V. M., Harris, T. M., and Stone, M. P. (1993) *Chem. Res. Toxicol. 6*, 64−68.
29. Iyer, R. S., Coles, B. F., Raney, K. D., Thier, R., Guengerich, F. P., and Harris, T. M. (1994) *J. Am. Chem. Soc. 116*, 1603−1609.
30. Bailey, E. A., Iyer, R. S., Harris, T. M., and Essigmann, J. M. (1996) *Nucleic Acids Res. 24*, 2821−2828.
31. Bailey, E. A., Iyer, R. S., Stone, M. P., Harris, T. M., and Essigmann, J. M. (1996) *Proc. Natl. Acad. Sci. U.S.A. 93*, 1535−1539.
32. Gopalakrishnan, S., Harris, T. M., and Stone, M. P. (1990) *Biochemistry 29*, 10438−10448.
33. Gopalakrishnan, S., Liu, X., and Patel, D. J. (1992) *Biochemistry 31*, 10790−10801.
34. Jones, W. R., Johnston, D. S., and Stone, M. P. (1998) *Chem. Res. Toxicol. 11*, 873−881.
35. Giri, I., Jenkins, M. D., Schnetz-Boutaud, N. C., and Stone, M. P. (2002) *Chem. Res. Toxicol.* (in press).
36. Johnston, D. S., and Stone, M. P. (1995) *Biochemistry 34*, 14037−14050.
37. Green, C. L., Loechler, E. L., Fowler, K. W., and Essigmann, J. M. (1984) *Proc. Natl. Acad. Sci. U.S.A. 81*, 13−17.
38. Loechler, E. L., Green, C. L., and Essigmann, J. M. (1984) *Proc. Natl. Acad. Sci. U.S.A. 81*, 6271−6275.
39. Basu, A. K., and Essigmann, J. M. (1988) *Chem. Res. Toxicol. 1*, 1−18.
40. Johnston, D. S., and Stone, M. P. (2000) *Chem. Res. Toxicol. 13*, 1158−1164.
41. Cheng, J. W., Chou, S. H., and Reid, B. R. (1992) *J. Mol. Biol. 228*, 1037−1041.
42. Nikonowicz, E. P., Meadows, R. P., Fagan, P., and Gorenstein, D. G. (1991) *Biochemistry 30*, 1323−1334.
43. Chou, S. H., Cheng, J. W., and Reid, B. R. (1992) *J. Mol. Biol. 228*, 138−155.
44. Nikonowicz, E. P., and Gorenstein, D. G. (1990) *Biochemistry 29*, 8845−8858.
45. Kan, L. S., Chandrasegaran, S., Pulford, S. M., and Miller, P. S. (1983) *Proc. Natl. Acad. Sci. U.S.A. 80*, 4263−4265.
46. Patel, D. J., Kozlowski, S. A., Ikuta, S., and Itakura, K. (1984) *Biochemistry 23*, 3207−3217.
47. Greene, K. L., Jones, R. L., Li, Y., Robinson, H., Wang, A. H., Zon, G., and Wilson, W. D. (1994) *Biochemistry 33*, 1053−1062.
48. Gao, X., and Patel, D. J. (1988) *J. Am. Chem. Soc. 110*, 5178−5182.
49. Li, Y., Zon, G., and Wilson, W. D. (1991) *Proc. Natl. Acad. Sci. U.S.A. 88*, 26−30.
50. Maskos, K., Gunn, B. M., LeBlanc, D. A., and Morden, K. M. (1993) *Biochemistry 32*, 3583−3595.
51. Brown, T., Leonard, G. A., Booth, E. D., and Chambers, J. (1989) *J. Mol. Biol. 207*, 455−457.
52. Brown, T., Hunter, W. N., Kneale, G., and Kennard, O. (1986) *Proc. Natl. Acad. Sci. U.S.A. 83*, 2402−2406.
53. Hunter, W. N., Brown, T., and Kennard, O. (1986) *J. Biomol. Struct. Dyn. 4*, 173−191.
54. Schurter, E. J., Yeh, H. J. C., Sayer, J. M., Lakshman, M. K., Yagi, H., Jerina, D. M., and Gorenstein, D. G. (1995) *Biochemistry 34*, 1364−1375.
55. Yeh, H. J. C., Sayer, J. M., Liu, X., Altieri, A. S., Byrd, R. A., Lakshman, M. K., Yagi, H., Schurter, E. J., Gorenstein, D. G., and Jerina, D. M. (1995) *Biochemistry 34*, 13570−13581.
56. Schwartz, J. L., Rice, J. S., Luxon, B. A., Sayer, J. M., Xie, G., Yeh, H. J., Liu, X., Jerina, D. M., and Gorenstein, D. G. (1997) *Biochemistry 36*, 11069−11076.
57. Murray, R. W., and Jeyaraman, R. (1985) *J. Org. Chem. 50*, 2847−2853.
58. Piotto, M., Saudek, V., and Sklenar, V. (1992) *J. Mol. Biol. 6*, 661−665.
59. Arnott, S., and Hukins, D. W. L. (1972) *Biochem. Biophys. Res. Commun. 47*, 1504−1509.
60. Arnott, S., and Hukins, D. W. L. (1973) *J. Mol. Biol. 81*, 93−105.
61. Frisch, M. J., Trucks, G. W., et al. (1998) *Gaussian 98*, Gaussian Inc., Pittsburgh, PA.
62. Bayly, C. I., Cieplak, P., Cornell, W. D., and Kollman, P. A. (1993) *J. Phys. Chem. 40*, 10269−10280.
63. Borgias, B. A., and James, T. L. (1990) *J. Magn. Reson. 87*, 475−487.
64. Keepers, J. W., and James, T. L. (1984) *J. Magn. Reson. 57*, 404−426.
65. James, T. L. (1991) *Curr. Opin. Struct. Biol. 1*, 1042−1053.
66. Brunger, A. T. (1992) in *X-PLOR Version 3.1. A system for X-ray Crystallography and NMR*, Yale University Press, New Haven, CT.
67. Clore, G. M., Gronenborn, A. M., Carlson, G., and Meyer, E. F. (1986) *J. Mol. Biol. 190*, 259−267.
68. Ryckaert, J.-P., Ciccotti, G., and Berendsen, H. J. C. (1977) *J. Comput. Phys. 23*, 327−341.
69. Jorgensen, W. L., Chandrasekhar, J., Madura, J. D., Impey, R. W., and Klein, M. L. (1983) *J. Chem. Phys. 79*, 926−935.

70. Case, D. A., Pearlman, C. A., et al. (1999) *AMBER 6.0*, University of California, San Francisco, CA.
71. Cornell, W. D., Cieplak, P., Bayly, C. I., Gould, I. R., Merz, K. M., Ferguson, D. M., Spellmeyer, D. C., Fox, T., Caldwell, J. W., and Kollman, P. A. (1995) *J. Am. Chem. Soc. 117*, 5179.
72. Darden, T., York, D., and Pedersen, L. (1993) *J. Chem. Phys. 12*, 10089−10092.
73. Essmann, U., Perera, L., Berkowitz, M. L., Darden, T., Lee, H., and Pedersen, L. G. (1995) *J. Chem. Phys. 103*, 8577−8593.
74. Allain, F. H., and Varani, G. (1997) *J. Mol. Biol. 267*, 338−351.
75. Mauffret, O., Amir-Aslani, A., Maroun, R. G., Monnot, M., Lescot, E., and Fermandjian, S. (1998) *J. Mol. Biol. 283*, 643−655.
76. Lu, X. J., Shakked, Z., and Olson, W. K. (2000) *J. Mol. Biol. 300*, 819−840.
77. Reid, B. R. (1987) *Q. Rev. Biophys. 20*, 2−28.
78. Patel, D. J., Shapiro, L., and Hare, D. (1987) *Q. Rev. Biophys. 20*, 35−112.
79. Boelens, R., Scheek, R. M., Dijkstra, K., and Kaptein, R. (1985) *J. Magn. Reson. 62*, 378−386.
80. Rinkel, L. J., and Altona, C. (1987) *J. Biomol. Struct. Dyn. 4*, 621−649.
81. Rein, R., Shibata, M., Garduno-Juarez, R., and Kieber-Emmons, T. (1983) in *Structure and Dynamics: Nucleic Acids and Proteins* (Clementi, E., and Sarma, R. H., Eds.) pp 269−288, Adenine Press, New York.
82. Egli, M., Williams, L. D., Frederick, C. A., and Rich, A. (1991) *Biochemistry 30*, 1364−1372.
83. Frederick, C. A., Williams, L. D., Ughetto, G., Van der Marel, G. A., Van Boom, J. H., Rich, A., and Wang, A. H. J. (1990) *Biochemistry 29*, 2538−2549.

BI012116T